RSC Advances

ROYAL SOCIETY OF CHEMISTRY

www.rsc.org/advances

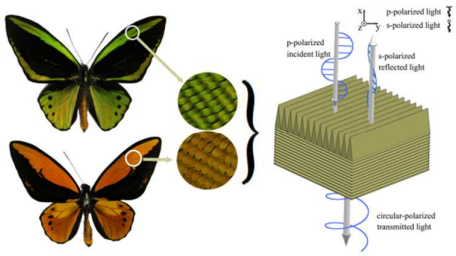

A combined architecture consisting of deep grating and multilayer in butterfly iridescent scales leads to the polarization-sensitive color.

Cite this: DOI: 10.1039/c0xx00000x

www.rsc.org/xxxxxx

ARTICLE TYPE

Polarization-sensitive color in iridescent scales of butterfly *Ornithoptera*

Ke Zhang [a], Shujun Zhou [a], Yiwen Tang [a], Ge Wang [b], Han Zhou [a], Tongxiang Fan* [a], Di Zhang [a]

Received (in XXX, XXX) Xth XXXXXXXXX 20XX, Accepted Xth XXXXXXXXX 20XX
DOI: 10.1039/b000000x

Diverse biological microstructures that result in advanced optical effects have been systematically investigated. However, the mechanisms of polarization-sensitive color have not been fully understood. Here we report a combined architecture comprised of upper deep grating and bottom multilayer in butterfly iridescent scales that leads to the polarization-sensitive color related with scale azimuth. The polarization process is unraveled through detailed investigations on the green scales in butterfly *Ornithoptera priamus poseidon* and the orange scales in butterfly *Ornithoptera croesus lydius*. The bright green and orange scales result from the interaction between the transmitted *0th* order diffraction of upper grating and the *1st* order interference of the bottom multilayer. Combining experiment with calculation, we clarify the structural origin and the mechanism of the polarization conversion. Tapered grating achieves form-birefringence rotating polarized light, and the multilayer selectively reflects the incident light dominating the reflection color. The height of the grating, which determines the phase difference of the two decomposed polarized lights, is essential to the polarization conversion. To our knowledge, it is the first time to provide a structural prototype comprised of deep grating and multilayer for achieving polarization-sensitive color. These findings show great promise in bio-sensing, anti-counterfeiting and optical-material design.

Introduction

Many natural biological structures achieve structural colors, the mechanisms of which inspire bio-mimetic photonic materials [1-7]. The natural organisms usually adopt typical ordered structures, such as grating, multilayer, and photonic crystals, to produce ordinary color signals like iridescence [8-10]. However, more elaborate microstructures are required to achieve sophisticated optical effects such as the polarization-sensitive color [11-14]. The *Chrysina gloriosa* beetle adopts the chiral and periodic helical structures to selectively reflect the left-circularly polarized light to have a striking iridescence[11]. The fruit of *Pollia condensate* has an intriguing pointillist appearance because of the helical structure in its surface that leads to a specific color [12]. The wings of *Papilio palinurus* butterfly and *Madagascan* sunset moth display a color mixing effect because of the retro-reflection structure that rotates the linearly polarized light [13, 14].

The polarization-sensitive color is caused by the polarization-dependent reflection and can increase the perceived visual contrast of light different with brightness and wavelengths [15]. Previous studies show that many organisms having polarization-sensitive photoreceptors can potentially discriminate objects through the polarization-dependent reflectance [16, 17]. The polarized light signals contribute to the biological signalling functions in mating, feeding, and oviposition [18-20]. For example, the *Papilio aegeus* and *Heliconius* butterflies use the polarized light in mate recognition [18]. Utilizing the polarized light signals is highly useful for species living in complex light environments [20], where illumination can dramatically change in brightness and spectral properties.

Here we report a polarization-sensitive phenomenon in the butterfly *Ornithoptera* iridescent scales. Detailed investigations on the green scales of butterfly *Ornithoptera priamus Poseidon* (*O.p.poseidon*) and the orange scales of butterfly *Ornithoptera croesus lydius* (*O.c.lydius*) reveal the structural origin of the polarization-sensitive color. Combined architecture comprised of upper deep grating and bottom multilayer is extracted from scale structure for unraveling the polarization mechanism. Through experiments and calculations, we clarify that the combined architecture selectively reflects and rotates incident polarized light.

Material and methods

Butterfly Samples

The investigated *O.p.poseidon* and *O.c.lydius* male butterflies, two species of the bird-wing butterfly living in Indonesia, were provided by the Shanghai Entomological Museum, China.

[a] *State Key Lab of Composites, Shanghai Jiaotong University, Shanghai 200240, P.R. China. E-mail: txfan@sjtu.edu.cn; Fax: +86-21-34202497; Tel: +86-21-54747779*
[b] *Instrumental Analysis Center, Shanghai Jiaotong University, Shanghai 200240, P.R. China*
**Corresponding author*
†Electronic Supplementary Information (ESI) available.

Cite this: DOI: 10.1039/c0xx00000x

www.rsc.org/xxxxxx

ARTICLE TYPE

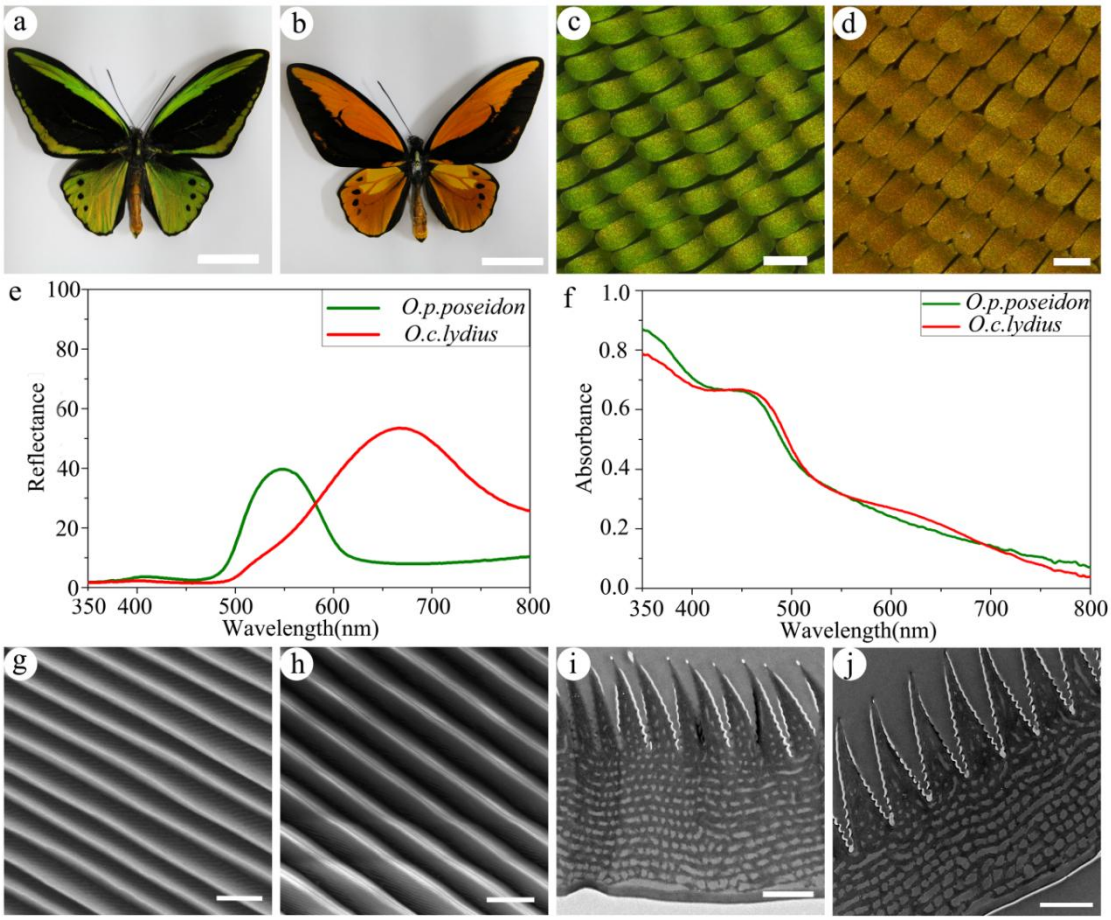

Fig. 1 Morphology and spectra of *O.p.poseidon* green scales and *O.c.lydius* orange scales. (a) Photograph of *O.p.poseidon* dorsal surface. (b) Photograph of *O.c.lydius* dorsal surface. (c) Optical microscopic image of green scales. (d) Optical microscopic image of orange scales. (e) Reflectance spectra tested with an integrating sphere. (f) Normalized absorption spectra of single scale immersed in bromoform (g) FESEM image of green scale from the top view. (h) FESEM image of orange scale from the top view. (i) TEM image of the cross-section of green scale. (j) TEM image of the cross-section of orange scale. Scales bar: (a, b) 2cm; (c-d) 100μm; (g-j) 1μm.

Morphology characterization

Digital photographs were captured by Canon EOS 350D digital camera. Optical microscopic images were obtained with a digital microscope (VHX-100, KEYENCE), revealing the arrangement of butterfly wing scales. The polarization effect was investigated on the Zeiss Axio Scope A1 Microscope equipped with collinear and crossed polarizers. The anatomical microstructure of wing scales was investigated with field emission scanning electron microscope (FESEM; FEI NOVA NanoSEM 230) and transmission electron microscopy (TEM; FEI Tecnai G2 spirit Biotwin). Samples for TEM imaging were prepared by first embedding the wing scales in epoxy resin at 60 ℃ for 48 hours, then cutting with a low temperature sectioning system (Leica ULTRACUT UC6) into ultrathin sections (70 nm), and finally staining with lead citrate for 6 minutes.

Spectra

The reflectance spectra of intact wings were measured with a normal UV-Vis-NIR spectrometer (Varian Cary 500 infrared-visible-ultraviolet spectrometer with an integrating sphere) and 1 cm^2 area of forewing color patches were subjected to the incident light. To obtain the absorbance spectrum of the absorbing pigments within the wing scales with micro-spectrophotometer (Craic QDI 2010), color scales were removed with adhesive tape. A single scale was immersed in bromoform, whose refractive index (RI) is 1.6 [21], and 10 μm^2 area of a single scale was illuminated by the incident light. Angle-dependent reflectance spectra were collected using an UV–Vis–IR fiber optical spectrometer (Ideaoptics Instruments Ltd., China). The incident light illuminated on the intact color scales and the diameter of the circular light spot was about 2 mm. The incident light and

detector were rotated in the plane perpendicular to the scales to measure the mirror angles. To investigate the polarization-dependent reflection, we equipped the fiber optical spectrometer on the Zeiss Axio Scope A1 Microscope. The diameter of the circular light spot was about 40 μm. Upon the crossed polarizers and the collinear polarizers, we rotated the sample azimuth to obtain the polarization-dependent reflectance spectra.

Chromaticity diagram

The chromaticity coordinates x and y were calculated by the formula as defined by the CIE 1931 convention [2].

Simulated calculation

Theoretical simulations were performed on software OptiFDTD from Optiwave Systems Inc. According to the parameters obtained from the FESEM and TEM images, we established the simplified scale model. For Finite Difference Time Domain (FDTD) simulation, a Gaussian modulated light source was adopted. Anisotropic perfect matching layer (APML) boundary condition was employed. The resulting calculation data was transferred from time domain to frequency domain by discrete Fourier transform method, generating the simulated spectra.

Results and discussion

Wing morphology and Optical spectra

The two sister species of butterfly *Ornithoptera*, *O.p.poseidon* and *O.c.lydius*, have different dorsal wing patches. The butterfly *O.p.poseidon* exhibits striking green patterns, while the butterfly *O.c.lydius* has orange patterns (Fig. 1a, b). The *O.p.poseidon* and *O.c.lydius* forewings both have cover scales of about 140 μm in length and 80 μm in width, which closely pack on the black ground scales (Fig. 1c, d).

Reflectance spectra were measured on spectrophotometer with an integrating sphere at normal incident light. The green and orange scales have a reflectance peak at 550 nm and 670 nm, respectively, as show in Fig. 1e. In order to identify the pigments in the scales, we investigated the absorption spectra of the pigments in the green and orange scales. A single green scale, and a single orange scale were immersed in bromoform (RI is1.6), approximately matching the RI of chitin (RI is 1.56)[21]. The absorbance spectra of both wing scales have similar main bands in the violet-blue wavelength range from 350 nm to 480 nm (Fig. 1f), suggesting that the pigments in both the green and orange scales have similar light-absorbing effects.

The FESEM and TEM images reveal the similar structures of the green and orange scales (Fig. 1g-j). Tapered ridges, with tiny inclination cross-ribs, run parallel to the longitudinal axis of the scale. The adjacent distance of the ridges is 0.54 μm for green scale and 0.76 μm for orange scale (Fig. 1g, h). Images of the cross-section perpendicular to the longitudinal axis of scale show anatomical architecture consisting of upper tapered ridges and bottom multilayer (Fig. 1i, j). In the green scales, the tapered ridges structure is 1.90 μm and the multilayer is 2.50 μm in height. In the orange scale, the tapered ridges structure is 2.60 μm and the multilayer is 2.60 μm in height. The bottom multilayer structure is comprised of alternative chitin and hybrid layers (hybrid layer is comprised of chitin columns and air). The thickness of the chitin layer is about 0.10 μm and the thickness of hybrid layer is about 0.11 μm for green scale, and 0.12 μm and 0.14 μm, respectively, for orange scale (Fig.S1, ESI†). A schematic model of the scale structure was established, and the average dimensions of which were statistically determined based on FESEM and TEM images. (Fig.S2a, ESI† and Table S1, ESI†). This model was further simplified to facilitate analysis on the optical effects in the green and orange scales (Fig.S2b, ESI†). The tapered ridges structure was simplified into tapered triangular grating structure, and the bottom multilayer structure (alternative chitin and hybrid layers) was simplified into ideal multilayer structure (Fig.S2b, ESI†). The optical mechanism was analyzed based on the simplified architecture comprised of an upper grating structure and a bottom multilayer structure.

Table 1 Effective RI of the grating and the hybrid layer

butterfly	*O.p.poseidon*		*O.c.lydius*	
structure	hybrid layer	grating	hybrid layer	grating
chitin volume ratio	0.11	0.9	0.06	0.80
effective RI	1.08	1.50	1.04	1.48

The RI of chitin and air are 1.56 and 1.00, respectively[21]. According to the parameters of the scales (Table S1, ESI†) and the effective RI theory [10],

$$n = \sqrt{f_c\, n_c^2 + (1-f_c) n_{air}^2} \quad (1)$$

Where n_c and n_{air} is the RIs of chitin and air, and f_c is the volume ratio of the chitin. The calculated effective RIs of the every part in the combined architecture are shown in Table 1 (Fig.S2b, ESI†).

When the normal incident light illuminates on the combined architecture, the upper triangular grating should cause the grating diffraction and the bottom multilayer should cause the multilayer interference [22]. The grating diffraction and multilayer interference orders was calculated to explain the optical phenomenon in the *O.p.poseidon* and *O.c.lydius* butterflies.

It has been shown that the tapered triangular grating acts as an antireflection layer that reduces the reflected diffraction order [23]. In our model, the grating has adjacent distance comparable with the wavelength of visible light, therefore the modal-method is effective for interpreting the diffraction behavior [24, 25.] According the modal-method, only the transmitted $0th$ order and $\pm 1st$ orders diffraction lights ($0th$ and $\pm 1st$ mode lights) will be non-evanescent at normal incident light [24-26]. The $0th$ and $\pm 1st$ mode lights pass through the upper grating, and then reach the bottom multilayer in the $0th$ and $\pm 1st$ transmitted diffraction angles, respectively.

In the case of the $0th$ mode light, the $0th$ transmitted diffraction angle is zero. The $0th$ mode light normally reaches the bottom multilayer and causes the optical coherent interference. The constructive interference equation of multilayer is given by [22],

$$n_c t_c \cos\theta_c + n_h t_h \cos\theta_h = \frac{m\lambda}{2} \quad (2)$$

where n_c (n_h), t_c (t_h), and θ_c (θ_h) are the RI, the thickness, and the refractive angle of the chitin layer (hybrid layer), and λ is the incident light wavelength and m is integer.

Cite this: DOI: 10.1039/c0xx00000x

www.rsc.org/xxxxxx

ARTICLE TYPE

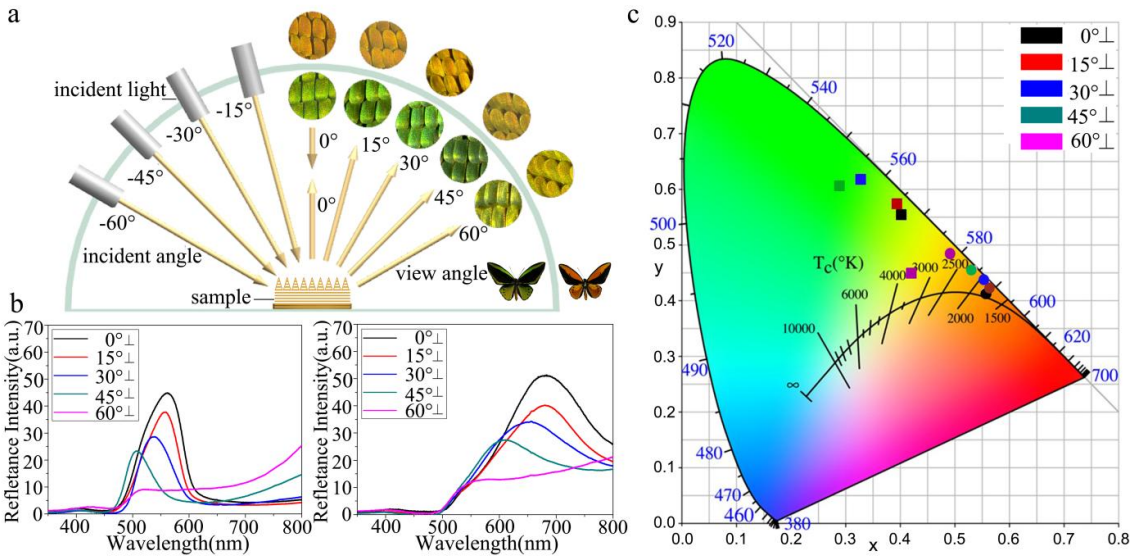

Fig.2 Iridescence property of green scales and orange scales. The incident light and detector rotate in the plane perpendicular to the scale ridge to measure the mirror angles. (a) Angle-dependent optical microscopic images of green and orange scales. (b) Angle-dependent reflectance spectra of green and orange scales. (c) Chromaticity diagram of the angle-dependent reflectance spectra in green and orange scales. The square represents the corresponding color of green scales, and the circle represents the corresponding color of orange scales. "⊥" represents that incident light and detector rotate in the plane perpendicular to the scale ridges.

The calculation peak of the multilayer is at 550 nm and 670 nm (m=1) in the green and orange scales, respectively. The experimental reflectance peaks (Fig. 1e) are approximately the same with the results of the 1st order multilayer interference of the 0th mode light, indicating that the 0th mode light contribute to the striking color of the green and orange scales.

In the case of the $\pm 1st$ mode lights, the incident lights reach the multilayer in the diffraction angles, $\theta_{\pm 1} = \frac{\pm\lambda}{n_c d}$, respectively [24].

The relevant calculation is shown in TextS1, ESI†. According the multilayer interference theory, the obtained calculated peaks of the multilayer are at 410 nm and 550 nm (m=1) in green and orange scales, respectively, which are shorter than the experimental results (Fig.S4, ESI†). Therefore, the $\pm 1st$ mode lights should have little contribution to the main bands of the reflectance spectra. The reflected lights of the transmitted $\pm 1st$ diffraction order of the green scales are probably suppressed by the pigment, which has a main absorbance band from 350nm to 480nm). The reflected lights of the transmitted $\pm 1th$ diffraction orders in the orange scale slightly widen the reflection range.

Theoretical calculation based on our model indicates that the main reflection bands of the green and orange scales mainly result from the interaction between transmitted 0th order diffraction of the grating and the 1st order interference of the multilayer.

Iridescence of the green and orange scales

In nature, iridescence is a structural color widely observed in birds, beetles, and butterflies. Iridescence is known to depend on the incident light and viewing angle. Multilayer interference iridescence has been found in the elytra of the jewel beetle *Chrysochroa fulgidissima* and the breast-feather barbules of the bird *Parotia lawesii* [27-29].

Fig. 2 shows angle-dependent optical microscopic images and reflectance spectra in the plane perpendicular to ridges. The incident light and detector are rotated in the plane perpendicular to the scale ridges to achieve different mirror angles. The observed color of the green scales gradually changes from yellowish green to bluish green with the increasing viewing angle, and becomes yellow at 60 º. In the case of the orange scales, the observed color gradually changes from orange to yellow (Fig. 2a). The peaks of angle-dependent reflectance spectra of both butterflies undergo blue shift with increasing viewing angle, and vanish at 60 º (Fig. 2b). The chromatic diagram confirms the relation between the color variation and reflectance spectrum, revealing that the yellow color at 60 º is caused by the disappearance of the spectrum peaks. The tendency of color variation in chromatic diagram is the same as that in experimental microscopic images (Fig. 2c).

Both angle-dependent spectra show blue shift tendency with the increasing of incident angle (Fig. 2b). Their reflectance amplitudes decrease with the increasing of incident angle, which is similar to the angle-dependent spectra of the breast-feather barbules in *Lawes' parotia* [28, 29]. However, for the classical multilayer, the reflectance amplitude will increase with the increasing angle of incidence [27, 28]. Thus, the upper tapered ridges probably affect the reflectance of the bottom multilayer under oblique incidence, and lead to the reflectance amplitude different

form that of the classical multilayer. The vanishing of peaks at 60 º in reflectance spectra may be caused by imperfect structures of the wing scales, such as disordered array and curvature. The valley from ultraviolet to about 480nm in reflectance spectra, which keeps low reflection, is strongly suppressed by pigment filter [30].

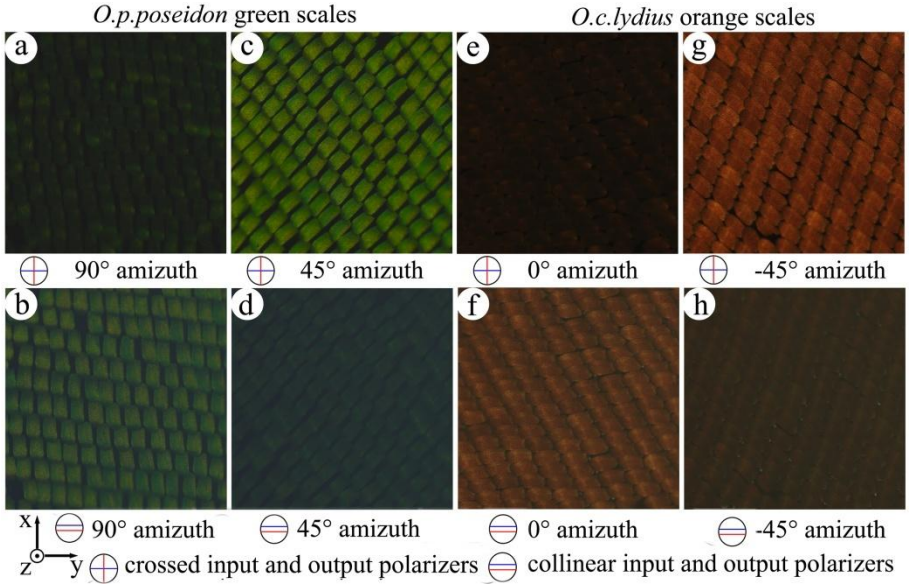

Fig. 3 Polarization property of green scales and orange scales (a) Green scales at 90º azimuth under crossed polarizers (b) Green scales at 90 º azimuth under collinear polarizers (c) Green scales at 45º azimuth under crossed polarizers (d) Green scales at 45º azimuth under collinear polarizers (e) Orange scales at 0º azimuth under crossed polarizers (f) Orange scales at 0º azimuth under collinear polarizers (g) Orange scales at -45º azimuth under crossed polarizers (h) Orange scales at -45º azimuth under collinear polarizers.

Structural Origin and Mechanism of Polarization

Optical microscopic images under the polarization microscope reveal that the green and orange scales have the polarization-sensitive effect dependent on the scale azimuth (Fig. 3). The scale under the crossed and collinear analyzers was observed with the orientation of the input linear polarizer fixed. The scale was rotated to investigate its polarization-sensitive property. The input linear polarizer and the collinear analyzer are parallel to the *y* coordinate axis, and the crossed analyzer is parallel to the *x* coordinate axis. Under the crossed analyzer, the reflected light almost extinguishes when the scale ridges are perpendicular or parallel to the input linear polarizer (Fig. 3a, e).While, it reappears when the scale rotates ±45 ºto the input linear polarizer (Fig. 3c, g). Under the collinear analyzer, the reflected light fades when the scale ridges are at ±45 º azimuth (Fig. 3d, h). The reflected light mainly transmits through the collinear analyzer, when the scale ridges are at 0 ºor 90 ºazimuth (Fig. 3b, f). Notably, the scales under polarized light exhibit colors different from those under non-polarized light.

A fiber optical spectrometer was equipped on the Zeiss Axio Scope A1 Microscope to collect the reflectance spectra to investigate the polarization-dependent reflection of the scales. The input linear polarizer is parallel to the *y* axis, the angle between scale ridges and input linear polarizer was 45 º(Fig. 4a). Here, the polarized orientation of p-polarized light is parallel to the *y* coordinate axis and the polarized orientation of s-polarized light is parallel to the *x* coordinate axis. Under the crossed polarizers, the s-polarized reflection bands are at 500-600 nm and 650-730 nm in the green and orange scales, respectively. Under the collinear polarizers, the p-polarized reflectance of the green and orange scales is approximately less than 5% (Fig. 4b). The polarization-dependent reflected spectra reveal that when the scale is at the 45 ºazimuth, it selectively reflects the incident light and rotates the p-polarized incident light into s-polarized light.

Previous studies show that polarized light can be caused by differential reflection or differential scattering, double reflection, or differential absorption [31, 32]. To demonstrate that the polarization conversion is caused by the anisotropic ridge structure rather than the pigments, we set the imaginary part of the material's RI to zero to eliminate the influence of pigments.

The normal incident light is a p-polarized light, and the combined architecture is at 45 ºazimuth (Fig. 4a). Simulation was performed with FDTD, and the calculated reflectance spectra are shown in Fig. 4c. The simulated s-polarized reflectance spectra show a reflection band at about 460-640 nm with the green scale model and a reflection band at about 570-730 nm with the orange scale model. Both the calculated p-polarized reflectance with the green and orange scale models is approximately less than 10%. Although the calculated s-polarized reflection bands with the green and orange scale models are wider than their experimental counterparts, both the calculated and experimental s-polarized reflection bands exhibit the same polarization conversion property, suggesting that the polarization conversion should be mainly caused by the anisotropic ridges structure.

To further clarify the polarization conversion progress caused by the scale model (45 º azimuth), we analyzed the optical process using the form-birefringence. Here we only analyzed the 0*th* mode light because it has main contribution to the reflection band. Previous studies show that the triangular grating achieves form-birefringence, leading to non-symmetric effective RIs [33, 34].

Cite this: DOI: 10.1039/c0xx00000x

www.rsc.org/xxxxxx

ARTICLE TYPE

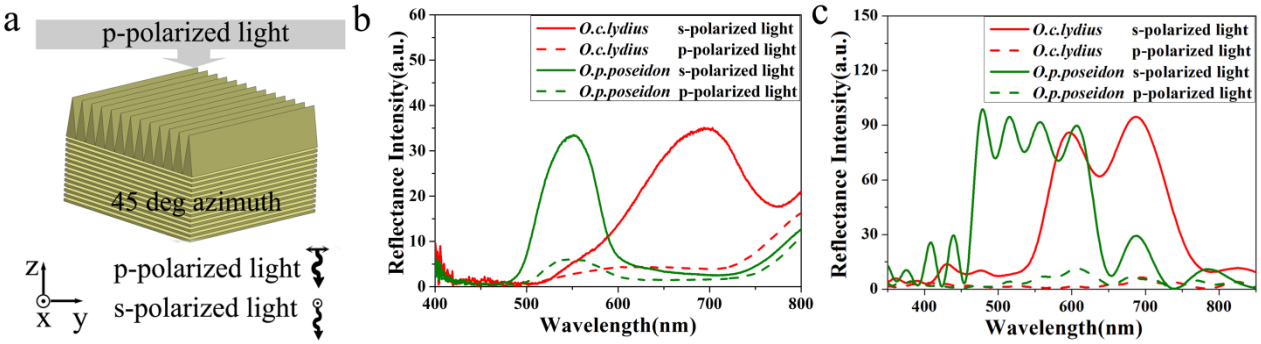

Fig. 4 Experimental and simulated polarization-dependent reflectance spectra of the 45º azimuth scale. (a) The 45º azimuth scale model. (b) The experimental polarization-dependent reflectance spectra of green and orange scales. (c) The simulated polarization-dependent reflectance spectra of green and orange scales.

The form-birefringence effective RI theory [33] is given by,

$$\begin{cases} n_{//}^2 = f n_r^2 + (1-f) n_{air}^2 \\ \dfrac{1}{n_{\perp}^2} = \dfrac{f}{n_r^2} + \dfrac{(1-f)}{n_{air}^2} \end{cases} \quad (3)$$

Where $n_{//}$ and $n_{\perp}$ are the effective RIs in the parallel and perpendicular grating orientation, respectively; f is the volume fraction, n_{air} is the RI of air, and n_r is the effective RI of ridge. The different effective RIs along parallel and perpendicular grating orientations should cause a phase difference. We decomposed the incident p-polarized light at normal incidence into two polarized light components, the parallel and perpendicular grating lights (Fig.S6, ESI†). The phase difference, δ_i, is described with the following equation

$$\delta_i = 2\int_0^{h_r} \frac{2\pi}{\lambda_i}(n_{//} - n_{\perp}) d_h \quad (4)$$

where λ_i is the wavelength of light, d_h is the infinitesimal segment in the tapered ridge, h is the distance from the infinitesimal segment to the top of ridge, h_r is the height of the ridge, $n_{//}$ and $n_{\perp}$ are the effective RIs along the parallel and perpendicular grating orientations. The relevant calculation is shown in TextS2, ESI†.

The s-polarized reflection intensity $I_{iR}(s)$ and the p-polarized reflection intensity $I_{iR}(\mathrm{p})$ are given by [35],

$$\begin{cases} I_{iR}(s) = I_{i0} R_i \sin^2(\dfrac{\delta_i}{2}) \\ I_{iR}(\mathrm{p}) = I_{i0} R_i \cos^2(\dfrac{\delta_i}{2}) \end{cases} \quad (5)$$

where λ_i is the wavelength, and I_{i0} is the intensity of incident p-polarized light, and R_i is the reflectance of multilayer. The relevant calculation is shown in TextS3, ESI†. The obtained results show that $I_{iR}(s) = I_{i0} R_i \sin^2(0.25\pi/\lambda_i)$ for green scale and $I_{iR}(s) = I_{i0} R_i \sin^2(0.32\pi/\lambda_i)$ for orange scale. The values of the $\sin^2(\delta_i/2)$ approximately match those of R_i in both the green and orange scales, suggesting that the height of the grating may be essential for the polarization-dependent reflection. These calculated results can well explain our experimental observations that the color of the 45 ºazimuth scales is intense under the crossed analyzer (Fig. 3c,g) while it dims under the collinear analyzer (Fig. 3d,h).

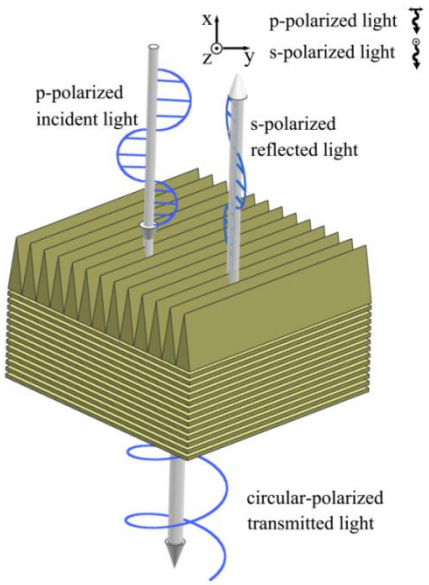

Fig. 5 Schematic diagram of polarization conversion process. When the p-polarized incident light illuminates on the 45º azimuth scale model, the reflected light is s-polarized light, and the transmitted light is circular-polarized light.

When the linearly polarized light illuminates on the 45 º azimuth quarter-wave plate, the transmitted light will be circular polarized [36]. In our model, the upper triangular grating acts as a quarter-wave plate. When p-polarized light illuminates on the 45 º azimuth simplified model, the transmitted light will be circular polarized. While, our study

reveals that the reflected light will be s-polarized. Therefore, the whole combined architecture at 45° azimuth selectively reflects and rotates the incident p-polarized light into the s-polarized light (Fig. 5).

Conclusions

The iridescent scales of two *Ornithoptera* butterflies, *O.p.poseidon* and *O.c.lydius*, exhibit a polarization conversion phenomenon at 45° azimuth, which is caused by an elaborate architecture consisting of tapered ridges covering a multilayer in the scale. The tapered ridge structure serves as triangular grating, which causes form-birefringence and hence different phases in different component lights, parallel and perpendicular grating lights, depending on the height of the triangular grating. The multilayer structure selectively reflects the incident light, contributing to the reflection band and deciding the intense color. The whole scale architecture consisting of the tapered ridges and the multilayer hence can selectively reflect and rotate the incident polarized light, leading to the polarization-dependent reflection and polarization-sensitive colors. These findings provide the design guide for bio-mimetic optical materials with polarization-sensitive structural colors, showing great promise in bio-sensing, anti-counterfeiting.

Acknowledgements

The authors are grateful for the financial support from the National Natural Science Foundation of China (51172141) and the Research Fund for the Doctoral Program of Higher Education (20100073110065 and 20110073120036).

References

1. E. Yablonovitch, *J. Mod. Optic.*, 1994, **41**, 173-194.
2. M. Srinivasarao, *Chem. Rev.*, 1999, **99,** 1935-1961.
3. A. R. Parker, Philos. *Trans. A Math. Phys. Eng. Sci.*, 2004, **362**, 2709-2720.
4. I.B. Burgess, J. Aizenberg, and M.Lončar. *Bioinspir. & biomim.*, 2013, **8(4)**, 045004.
5. M. Kolle, *Photonic structures inspired by nature*, Heidelberg: Springer; 2011, pp 30-55.
6. P-Y Chen, J. McKittrick and M. A. Meyers, *Prog. Mater. Sci.*, 2012, **57**, 1492-1704.
7. K. L. Yu, T. X. Fan, S. Lou and D. Zhang, *Prog. Mater. Sci.*, 2013, **58**, 825-873.
8. M. Kolle, A. Lethbridge, M. Kreysing, J. J. Baumberg, J. Aizenberg, and P.Vukusic, *Adv. Mater*, 2013, **25(15)**, 2239-2245.
9. A. R. Parker, *J. Exp. Biol.*, 1998, **201**, 2343-2347.
10. V. Saranathan, C. O. Osuji, S. G. J. Mochrie, H. Noh, S. Narayanan, A. Sandy, E. R. Dufresne and R. O. Prum, *Proc. Natl. Acad. Sci. USA*, 2010,**107**, 11676–11681.
11. V. Sharma, M .Crne, J. O. Park and M. Srinivasarao, Science, 2009, **325**, 449-451.
12. S. Vignolini, P. J. Rudall, A. V. Rowland, A. Reed, E. Moyroud, R. B. Faden, J. J. Baumberg, B. J. Glover and U. Steiner, *Proc. Natl Acad. Sci. USA*, 2012, **109**, 15712-15715.
13. P. Vukusic, J. R. Sambles and C. R. Lawrence, *Nature*, 2000, **404**, 457-457.
14. S. Yoshioka and S. Kinoshita, Opt Express, 2007, **15**, 2691-2701.
15. J. M. Douglas, T. W. Cronin, T. H. Chiou and N. J. Dominy. *J. Exp. Biol.*, 2007, **210(5)**, 788-799.
16. T.W. Cronin, N. Shashar, R.L. Caldwell, J. Marshall, A.G. Cheroske and T. H. Chiou, *Integr. Comp. Biol.*, 2003, **43**, 549-558.
17. S. Kleinlogel and A. G. White, *PloS one*, 2008, **3**, e2190.
18. A. Kelber, *Nature*, 1999, **402**, 251.
19. A. Kelber, C. Thunell and K. Arikawa, *J. Exp. Biol.*, 2001, **204**, 2469-2480.
20. A. Sweeney, C. Jiggins and S. Johnsen, *Nature*, 2003, **423**, 31-32.
21. H. L. Leertouwer, B. D. Wilts and D. G. Stavenga. *Optics express*, 2011, **19(24)**, 24061-24066.
22. S. Kinoshita, S. Yoshioka and J. Miyazaki. *Rep. Prog. Phys.* 2008, **71**, 076401.
23. S Lou, X. M. Guo, T. F. Fan and D. Zhang, *Enegr. Environ. Sci*, 2012, **5**, 9195-9216.
24. T. Clausnitzer, T. Kämpfe, E. B. Kley, A. Tünnermann, U. Peschel, A.V. Tishchenko and O. Parriaux, *Optics express*, 2005, **13(26)**, 10448-10456.
25. X. F. Jing, S. Z. Jin, J.C. Zhang, Y. Tian, P. Liang, H. B. Shu, L. Wang and Q. M. Dong, *Opt. Lett.*, 2013, **38**, 10-12.
26. A. V. Tishchenko, *Opt. Quant. Electron.*, 2005, **37**, 309-330.
27. D. G. Stavenga, B. D. Wilts, H. L. Leertouwer and T. Hariyama, *Philos. Trans. R. Soc. Lond. B Biol. Sci.*, 2011, **366**, 709-723.
28. D. G. Stavenga, H. L. Leertouwer, N. J. Marshall and D. sorio, *Proc. R. Soc. B*, 2011, **8**, 2098-2104.
29. B. D. Wilts, K. Michielsen, De Raedt H and D. G. Stavenga, *Proc. Natl. Acad. Sci. USA*, 2014, 111(12): 4363-4368.
30. B. D. Wilts, T. M. Trzeciak, P. Vukusic, D. G. Stavenga, *J. Exp. Biol.* 2012, **215**, 796-805.
31. G.P. Konnen, *Polarized light in nature*, Cambridge University Press; 1985, pp 131-143.
32. T. W. Cronin and J. Marshall. *Philos. Trans. R. Soc. Lond. B Biol. Sci.*, 2011, **366(1565)**, 619-626.
33. W. J. Yu, T. Konishi, T. Hamamoto, H. Toyota, T. Yotsuya and Y. Ichioka, *Appl. Opt.*, 2002, **41**, 96-100.
34. F. Wang, M. Xiao, K. Sun and Q. H. Wei, *Opt. Express*, 2010, **18**, 63-71.
35. Y. B. Liao, *Polarization optics*, Beijing Science press; 2003, pp 101-109.
36. C. Hitzenberger, E. Götzinger, M. Sticker, M. Pircher and A. Fercher, *Opt. Express*, 2001, **9**, 780-790.